Available online at www.sciencedirect.com
SCIENCE DIRECT®
Journal of volcanology and geothermal research
ELSEVIER
Journal of Volcanology and Geothermal Research 126 (2003) 263–283
www.elsevier.com/locate/jvolgeores

Phenocryst fragments in rhyolitic lavas and lava domes

S.R. Allen *, J. McPhie

Centre for Ore Deposit Research, University of Tasmania, Private Bag 79, Hobart, Tasmania 7001, Australia

Received 29 April 2002; accepted 24 April 2003

Abstract

Although rhyolitic lavas and lava domes are characterised by evenly porphyritic textures, not all the phenocrysts are whole euhedra. We undertook image analysis of 46 rhyolitic lava and lava dome samples to determine the abundance and shape of quartz and feldspar phenocryst fragments. Phenocryst fragments were identified in nearly all samples. On average, fragments amount to ~5% of the total phenocryst population, or ~0.5 modal%. The abundance of fragments in lavas and lava domes is not related to the groundmass texture (whether vesicular, flow banded, massive, glassy or crystalline), nor to distance from source. Fragments are, however, more abundant in samples with higher phenocryst contents. The phenocryst fragments in rhyolitic lavas and lava domes are mainly medium to large (0.5–3.5 mm), almost euhedral crystals with only a small portion removed, or chunky, equant, subhedral fragments, and occur in near-jigsaw-fit or clast-rotated pairs or groups. The fragments probably formed in response to decompression of large melt inclusions. Shear during laminar flow then dismembered the phenocrysts; continued laminar shear separated and rotated the fragments. Fractures probably formed preferentially along weaknesses in the phenocrysts, such as zones of melt inclusions, cleavage planes and twin composition planes. Rare splintery fragments are also present, especially within devitrified domains. Splinters are attributed to comminution of solid lava adjacent to fractures that were later healed. For comparison, we measured crystal abundance in a further 12 rhyolite samples that include block and ash flow deposits and ignimbrite. Phenocryst fragments within clasts in the block and ash flow samples showed similar shapes and abundances to those fragments within the lava and lava domes. Crystal fragments are much more abundant in ignimbrite (exceeding 67% of the crystal population) however, and dominated by small, equant, anhedral chunks or splinters. The larger crystals in the ignimbrite are subrounded. The phenocrysts within ignimbrite pumice lapilli are also more intensely fractured than those in lavas and lava domes. Thus, in deformed and altered volcanic successions, data on crystal fragment abundance and shape can help discriminate lavas from pyroclastic facies.

Keywords: lava; lava dome; rhyolite; phenocryst; phenocryst fragments; image analysis

1. Introduction

Most compositionally homogeneous lavas and lava domes are evenly porphyritic, and contain phenocrysts that are euhedral, and uniform in size, mineralogy and proportion throughout. A texture comprising evenly distributed, euhedral phenocrysts in a massive or flow-banded groundmass is considered typical of the products of effusive and very weakly explosive eruptions. In

* Corresponding author.
E-mail address: sharon.allen@utas.edu.au (S.R. Allen).

0377-0273/03/$ – see front matter © 2003 Elsevier Science B.V. All rights reserved.
doi:10.1016/S0377-0273(03)00151-3

comparison, broken crystals and uneven crystal distributions, together with vitroclastic matrix textures, are typical of the products of explosive eruptions (e.g. Branney et al., 1992; Best and Christiansen, 1997). Hence, in units that are poorly exposed or strongly affected by devitrification, recrystallisation, metamorphism, tectonic disruption or alteration, a dominance of evenly distributed, unbroken, euhedral crystals has been particularly useful for inferring an effusive origin (e.g. Allen, 1988; McPhie et al., 1993). Furthermore, some widespread felsic units, initially assumed to be ignimbrites, have been interpreted as extensive lavas in part because of evenly porphyritic textures (e.g. Bonnichsen and Kauffman, 1987; Manley, 1996a; Henry et al., 1988, 1990; Garner and McPhie, 1999; Allen and McPhie, 2002).

Use of the crystal population to distinguish a volcanic unit as pyroclastic or effusive requires knowledge of the usual abundance of phenocryst fragments in lavas and lava domes. Phenocryst fragments have been observed in lavas and lava domes, particularly in silicic examples (e.g. Ewart, 1968; Dadd, 1992; Manley, 1992, 1996b; Nakada et al., 1994; Burt et al., 1996). Their significance in lavas and lava domes has, however, largely been ignored and there is a lack of quantitative data on their abundance, type and size.

Crystals in porphyritic lavas and lava domes have a number of origins. The simplest origin of phenocrysts involves crystallisation from the melt prior to eruption (i.e. intratelluric crystals). Some phenocrysts may be derived from disintegration of crystalline wall rock (xenocrysts). In addition, phenocrysts may also be inherited from a crystal-rich 'mush' remaining from preceding eruptive episodes (e.g. Higgins, 1996; Nakagawa et al., 1999; Gamble et al., 1999; Cole et al., 2000; Eichelberger et al., 2000; Harford and Sparks, 2001). Porphyritic lavas and lava domes may also have crystals within the groundmass. Groundmass crystals result from syn-eruptive crystallisation of the magma (microlites; e.g. Swanson et al., 1989; Gibson and Naney, 1992) and/or crystallisation accompanying slow cooling from high temperature during and after emplacement (spherulites, micropoikilitic texture and granophyric texture; e.g. Lofgren, 1971).

In this paper, we present new data on the size and shape of feldspar and quartz phenocrysts within young, fresh rhyolitic lavas and lava domes, with the specific aim of quantifying the type and abundance of feldspar and quartz fragments. Rhyolites have been selected for this study as they show a marked distinction between the mm- to cm-size phenocrysts and the groundmass. Rhyolitic groundmass is mainly glassy, with or without microlites, or finely crystalline (<500 μm). Feldspar and quartz phenocrysts were measured as they are both the largest and the most abundant phenocryst phases in the rhyolites. These phases are also relatively durable, and can be recognised even in strongly altered and deformed rocks. The flow regime of rhyolitic lavas is laminar, reflecting their high viscosities (McBirney and Murase, 1984; Manley, 1992; Stevenson et al., 2001), and placing constraints on possible fragmentation mechanisms during outflow. We explore correlations among phenocryst size, abundance, sorting, groundmass textures, distance from source, and the presence of phenocryst fragments, and also discuss the implications for textural interpretation. Comparisons with new data on crystal fragments in rhyolitic ignimbrites allow consideration of the processes that lead to phenocryst fragmentation in silicic lavas.

1.1. Setting and character of samples

The rhyolitic lava and lava dome samples are predominantly from the Taupo Volcanic Zone (TVZ), New Zealand, with a few samples from Yali, Nisyros and Milos in the Hellenic arc (Greece). The majority of these lavas and lava domes are among the most recent products of their respective centres, and all are well preserved. Lavas are distinguished from lava domes according to their morphology: lava domes have $L/h \leq 5$ (where L = longest axis, h = thickness) and lavas have $L/h > 5$ (Stevenson et al., 1994).

The TVZ is a complex volcano-tectonic depression ca 300 km long and up to 60 km wide in the central North Island of New Zealand. It has been a focus of extensive and voluminous rhyolitic volcanism for the past ca 1.6 Ma (Wilson et al., 1995). Most of the rhyolitic magma has been ex-

pelled during caldera-forming explosive eruptions and eight calderas have been recognised. Numerous lavas and lava domes have been emplaced around or within the calderas. Three different volcanic centres within the TVZ were sampled for this study: Maroa, Okataina, and Kapenga (Table 1).

The lava dome samples of the Maroa volcanic centre come from the northwestern dome complex, the western dome complex and the Maroa volcano central dome, all of which post-date caldera formation (Wilson et al., 1986). The samples from the Kapenga volcanic centre come from the Moerangi and Tutakeheheke domes that represent the youngest activity of the centre, following eruptions of two inferred caldera-related ignimbrites (Rogan, 1982; Wilson et al., 1984; Wilson et al., 1995). The Okataina volcanic centre is the best exposed and best documented of the three centres (e.g. Nairn, 1981; Nairn and Wood, 1987). The lava and lava dome samples from the Okataina volcanic centre come from the Haroharo and Tarawera dome complexes that infill the large Haroharo caldera, with a few additional samples from lavas and lava domes that preceded caldera formation or lie outside the caldera margin (Nairn, 1989). The rhyolitic lavas and lava domes at the Okataina volcanic centre have typically followed explosive eruptions (Nairn, 1981).

During the ca AD 1305 Kaharoa eruptive episode at Tarawera, three summit lava domes were extruded and accompanied by voluminous block and ash flows (Nairn et al., 2001). Juvenile clasts from two of these block and ash flow sequences (Kaharoa and Wahanga) were also sampled. The block and ash flow clasts are porphyritic and vary in vesicularity from moderately vesicular breadcrust clasts with large (0.5–1.3 mm) spherical and coalesced vesicles, to almosy non-vesicular, perlitic clasts with scattered domains of very small (<20 μm) elongate vesicles.

The rhyolitic lavas and lava domes in the TVZ typically contain phenocrysts of plagioclase (oligoclase–labradorite), quartz, hypersthene, titanomagnetite, ilmenite, calcic hornblende, and in some cases biotite (Ewart and Healy, 1965; Ewart, 1968; Ewart et al., 1971, 1975). The ferromagnesian minerals in the rhyolitic lavas correlate with well-defined Fe–Ti oxide equilibration temperatures that range from 725 to 915°C (Ewart et al., 1971, 1975). Stevenson et al. (1994) found that the outflow extents of the Okataina rhyolitic lavas were related to the eruption volume, eruption rate, and pre-eruption ground surface morphology, as predicted by Walker (1973) and did not correlate with the crystallinity or viscosity. Stevenson et al. (1994) estimated the viscosity of these lavas to be in the order or 10^{10}–10^{11} Pa s.

Volcanism in the Hellenic arc began about 13 Ma ago in response to the complex collision between the African plate and the Eurasian plate (McKenzie, 1972). Milos is in the central part of the arc, whereas Nisyros and Yali are at the eastern end. All the samples are calc–alkaline rhyolite. The lava dome sampled on Milos lies on the northern coast and is Lower Pleistocene in age (Fytikas et al., 1986). Nisyros is a Quaternary cone volcano with a central caldera partly filled by several post-caldera silicic lava domes (Francalanci et al., 1995), two of which were sampled. The Yali lava domes occur on the northern part of the island, near or within the Kos Plateau Tuff caldera (Allen, 2001), and have been dated at 24 ka (fission track; Wagner et al., 1976). Plagioclase is the most common phenocryst phase, with lesser abundances of quartz, orthopyroxene, clinopyroxene, magnetite and hornblende, and very rare biotite (Francalanci et al., 1995).

The rhyolitic lavas and lava domes from the TVZ and Hellenic arc resemble the silicic lavas described by Christiansen and Lipman (1966) and show textural variations broadly similar to those identified in many other silicic lavas (e.g. Fink, 1983; Manley and Fink, 1987; Fink and Manley, 1987; Eichelberger et al., 1985). The carapace comprises fragments of obsidian that range from dense to moderately vesicular ($\sim$50 vol% vesicles) and includes extensive areas of coherent tube pumice. The pumiceous carapace grades inwards into non-vesicular obsidian. The groundmasses in the interior of the lava is crystalline. Obsidian also occurs at the base and may be non-vesicular, coherent and/or autobrecciated. The lava interior can be massive or show subtle, subhorizontal flow banding and widely spaced shrinkage joints.

Table 1
Location and textural characteristics of each sample

Number	Grid reference	Centre	Location	Caldera	Groundmass	Banded	Section cut		A	x	F	Density	Vesicles	A [a]	F [a]
	NZMS 260						with	cross	(modal%)	(%)	(modal%)	(g/cm^3)	(vol%)	recalc.	recalc.
24a	T17/585053	M	P	post	glassy	banded	1		<1						
24b	T17/585053	M	P	post	glassy	banded	1		1	11.0	0.11				
24c	T17/583062	M	P	post	pumiceous			1	<1	11.0					
25	T17/594065	M	P	post	glassy				1	10.0	0.1				
26	T17/654087	M	P	post	glassy	banded	1		1	14.0	0.14	2.2			
26b	T17/654087	M	P	post	pumiceous			1	1	0.2	0.001	1.67	24	1	0.001
22	U17/765868	M	P	post	pumiceous		1		20	1	0.2				
27	U17/736034	M	P	post	devitrified				15	4.8	0.72	2.22			
27b	U17/736034	M	P	post	pumiceous			1	23	4.8	1.10	1.76	21	28	1.34
19	V16/157237	O T	Pt	post	glassy	banded			21	2.5	0.53				
18d	V16/174247	O T	P i	post	pumiceous			1	19	6.4	1.22	1.58	31	25	1.59
18	V16/167241	O T	Pt	post	devitrified				24	3.5	0.84	2.3			
18b	V16/167241	O T	Pt	post	pumiceous		1		14	5.6	0.78	1.95	15	16	0.90
18b/2[b]	V16/167241	O T	Pt	post	pumiceous			1	14	3.7	0.52	1.9	17	16	0.61
20b	V16/181255	O T	P i	post	pumiceous		1		16	3.0	0.48	1.76	22	20	0.59
10 I	V16/165285	O T	D	post	glassy	banded			4	17.0	0.68	2.4			
10b	V16/165285	O T	D	post	pumiceous			1	3	5.0	0.15	1.4	42	4	0.21
11	V16/126268	O T	D	post	pumiceous		1		21	5	1.05	1.79	20	25	1.26
12	V16/124235	O T	D	post	glassy				17	7.0	1.19				
9	V16/159294	OH	D	post	glassy	banded	1		10	2.0	0.2				
4	V16/105368	OH	D	post	glassy/spherulitic	banded	1		11	12.0	1.32	2.16			
4a	V16/105368	OH	D	post	pumiceous			1	9	4.0	0.36	1.46	32	12	0.48
8	V16/142298	OH	D	post	glassy	banded		1	9	1.0	0.09				
8/2	V16/142298	OH	D	post	glassy	banded	1		10	3.0	0.3				
7	U16/095305	OH	D	post	glassy	banded		1	11	5.0	0.55				
7/2	U16/095305	OH	D	post	glassy	banded	1		11	5.0	0.55				
3	V16/106340	OH	D	post	glassy				11	19.0	2.09				
6	V15/118440	OH	D	post	glassy/microlitic	banded			6	13.0	0.78	2.3			
6b	V15/118440	OH	D	post	pumiceous			1	3	1.5	0.045	1.66	28	4	0.06
6b/2	V15/118440	OH	D	post	pumiceous		1		2	5.0	0.1	1.66	28	3	0.13
5	V16/108372	OH	D	post	glassy	banded	1		5	5.0	0.25	2.27			
5/2	V16/108372	OH	D	post	glassy	banded		1	5	12.0	0.6				
5b	V16/108378	OH	D	post	devitrified	banded	1		3	13.0	0.39				
5c	V16/108378	OH	D	post	pumiceous		1		3	3.0	0.09	1.45	36	4	0.12
15	U16/057275	OO	D	post	glassy	banded	1		10	11.0	1.1				
16b	U16/031274	OO	D	post	pumiceous			1	21	0.6	0.13				
14	U16/066276	OO	D	post	glassy	banded	1		11	4.0	0.44				
2d	V15/272426	O old	D	pre	devitrified						0				
17	U16/016315	O old	M	pre	devitrified/microlitic			1	17	5	0.85				
17/2	U16/016315	O old	M	pre	devitrified		1		12	5	0.6				
17b	U16/016315	O old	M	pre	devitrified		1		19	plucked					
									16		0				
IN24	U16/969269	KM	MD	post	pumiceous		1		16	0.5	0.08	1.6	28	20	0.10
IN31	U16/004280	KM	MD	post	pumiceous		1		14	4.0	0.56	1.51	33	19	0.74
IN28	U16/023281	KM	D	post	devitrified/spherulitic/microlitic				23	10.5	2.42				
IN30	U16/000288	KM	PM	post	devitrified				19	0.8	0.15				
IN20	U16/987323	KM	MD	post	glassy				13	3.0	0.39				
IN17	U16/991299	KM	MD	post	pumiceous		1		13	2.0	0.26	1.91	15	15	0.30
IN15	U16/989304	KM	MD	post	pumiceous		1		9	2.0	0.18	1.71	24	11	0.22
IN12	U16/995302	KM	M	post	spherulitic		1		12	1.0	0.12				
IN18	U16/999298	KM	M	post	devitrified				13	2.0	0.26				

Table 1 (*Continued*).

Number	Grid reference	Centre	Location	Caldera	Groundmass	Banded	Section cut		*A*	*x*	*F*	Density	Vesicles	*A* [a]	*F* [a]
	NZMS 260						with	cross	(modal%)	(%)	(modal%)	(g/cm^3)	(vol%)	recalc.	recalc.
IN21	U16/990324	KM	M	post	pumiceous		1		11	5.0	0.55	1.9	16	13	0.64
IN11	U16/033237	KT	MD	post	devitrified/spherulitic				16	5.0	0.8				
13	U16/081258	KT	D	post	devitrified				19	2	0.38				
13b	U16/081258	KT	D	post	pumiceous		1		18	5	0.9				
IN6	U16/016262	KT	MD	post	glassy	banded	1		16	4.0	0.64				
IN5	U16/023259	KT	M	post	devitrified/spherulitic		1		11	3.0	0.33				
In10	U16/059251	KT	M	post	glassy/spherulitic	banded			18	0.6	0.11				
IN37	U16/028240	KT	MD	post	spherulitic				20	3	0.6				
Y2a	Yali dome		P		glassy/spherulitic				3	8.0	0.24				
Y2b	Yali dome		P		glassy/spherulitic					13.0	0	2.3			
Y2c	Yali dome		P		glassy/spherulitic	banded			1		0	2.3			
Y1a	Yali dome		P		pumiceous/spherulitic		1		1	8.0	0.08	1.32	43	1	0.11
Y1b	Yali dome		P		pumiceous		1		1	6.0	0.06	1.77	23	1	0.07
N2a	Nisyros dome		P		glassy/microlitic		1		13	1.0	0.13	2.1			
N2a/b	Nisyros dome		P		glassy/microlitic		1		27	3.1	0.84				
N24a	Nisyros dome		P		pumiceous		1		17	3.0	0.51	1.7	18	20	0.60
N24b	Nisyros dome		P		pumiceous			1	14	3.0	0.42	1.98	5	15	0.44
N2b	Nisyros dome		P		pumiceous			1	26	1	0.26	2	3	27	0.27
M2	Milos dome		Pi		glassy	banded	1		6	3.0	0.18	1.88	14	7	0.21
M1	Milos dome		P		devitrified	banded			25	4.5	1.3	2.2			
Block and ash flow															
K1	V16/178195	OK			moderately vesicular, breadcrusted lapilli				5.1	27.6	1.40	1.17	48	7	2.07
K1b	V16/178196	OK			poorly vesicular, breadcrusted block				14.7	9.1	1.33	1.7	24	18	1.65
K1d	V16/178197	OK			incipiently vesicular				18.1	14.3	2.58	2.15	4	19	2.68
NZ1c	V16/218293	OW			non-vesicular				15.4	2.6	0.40	2.21			
NZ1d	V16/218294	OW			non-vesicular, perlitic obsidian				4.6	13.5	0.62				
NZ1f	V16/218295	OW			non-vesicular, perlitic				17.1	8.1	1.39				
NZ1g	V16/218296	OW			poorly vesicular				15.1	4.8	0.72	1.59	28	19	0.92
Ignimbrite															
NZL	T15/461614	Mg: Ongatiti ignimbrite			pumice clast				17.6	80.8	14.26	1	55	21	17.11
NZ	T15/461614	Mg: Ongatiti ignimbrite			pumice clast				17.8	84.0	14.98	1	55	21	17.98
A12p1	T15/461614	Mg: Ongatiti ignimbrite			pumice clast				11.9	67.5	8.04	1	55	15	10.29
A12p4	T15/461614	Mg: Ongatiti ignimbrite			pumice clast				8.4	78.6	6.60	1	55	10	8.19
A12	T15/461614	Mg: Ongatiti ignimbrite			matrix				25.2	85.2	21.44				
NZ	T15/461614	Mg: Ongatiti ignimbrite			matrix				23.8	95.5	22.67				

Centre: M, Maroa; O, Okataina; OT, Tarawera; OH, Haroharo; OK, Kaharoa; OW, Wahanga; OO, Okareka; O old, pre-date caldera; K, Kapenga; KM, Moerangi; KT, Tutakeheke; Mg, Mangakino. Location: P, proximal; Pi, interior; Pt, top; PM, proximal-medial; M, medial; MD, medial-distal; D, distal.

[a] *A*, *F*, recalculated modal% after conversion to dense rock.

[b] 18b/2: perpendicular sample to 18.

In addition to the lava, lava dome and block and ash flow samples, one ignimbrite (Ongatiti ignimbrite) from the TVZ was also selected for comparison. The 1.21 Ma rhyolitic Ongatiti ignimbrite was erupted from the Mangakino volcanic centre (Wilson et al., 1995). It is one of the largest (>300 km^3) ignimbrites erupted from the TVZ. The ignimbrite is slightly welded and glassy. The principal constituents are: coarsely porphyritic pumice lapilli, lithic lapilli, abundant free crystals and crystal fragments (plagioclase, quartz, orthopyroxene, hornblende, titanomagnetite, zircon, ilmenite, apatite), and glassy shards.

2. Methods

Forty-six different rhyolitic lavas and lava domes were sampled and analysed. In addition, we analysed a further 12 samples, including rhyolitic block and ash flow deposits from the Kaharoa eruptive episode, and pumice clasts and matrix from the Ongatiti ignimbrite. The authors collected 38 samples from the TVZ and four samples from domes in Greece. Ian Nairn (IGNS, New Zealand) contributed a further 16 samples from the Kapenga volcanic centre in the TVZ. Where possible, different parts of each lava or lava dome were sampled, including the pumiceous carapace, non-vesicular obsidian upper part and crystalline interior. Samples were also collected from the proximal (up to a few hundred metres from the vent), medial (within $\sim$1–2 km from the vent) and distal parts (at the margin) of single lavas and lava domes. A total of 76 thin sections were made of the lavas and lava domes (Table 1). For samples that were flow-banded, showed phenocryst alignment or had elongated vesicles, two perpendicular thin sections were made – one parallel and one at right angles to the foliation. None of the lavas or lava domes sampled show any obvious concentrations or depletions of phenocrysts at outcrop, hand specimen or in thin-section scales of observation. X-ray fluorescence (XRF) analyses of selected samples are shown in Table 2.

2.1. Image analysis

The thin sections were routinely magnified 6.3 or 10 times and photographed. Areas requiring greater detail were magnified up to 20 times. At least three and up to seven photomicrographs were taken to cover the area exposed on each thin section. Image analysis was undertaken on the photomicrographs to determine the size and abundance of feldspar and quartz phenocrysts. Size (perimeter) and length were determined for each phenocryst and averaged for each thin section. The length measure used is the maximum intersection length of the two-dimensional areas occupied by the phenocrysts.

The image analysis data for a two-dimensional section of a porphyritic sample dominated by triclinic (plagioclase) and trigonal (quartz) phenocrysts show a relatively clear correlation between length and perimeter (Fig. 1a): the perimeter is three times the size of the length. The relationship also holds for the average phenocryst length and perimeter in a sample: the average perimeter is also three times the average length (Fig. 1b). Phenocryst size sorting (standard deviation) was determined for each sample by first calculating the number of phenocrysts that fell into various perimeter size intervals. The size intervals were determined by the function $\log_2 p$, p being the perimeter in mm (e.g. size intervals 0.625–0.125, 0.125–0.25, 0.25–0.5... mm). The standard deviation of the phenocryst size distribution was then calculated and used as measure of sorting. Poorly sorted samples have high standard deviations and hence, high values for the sorting parameter. Sorting correlates only broadly with the average length: samples are poorer sorted as the average length of the phenocrysts increases (Fig. 1c).

Phenocryst contents of pumiceous samples (lavas, lava domes, breadcrust clasts from block and ash flow deposits, ignimbrite pumice) were recalculated for dense rock equivalents. The densities of pumiceous samples were determined by measuring their dry weight and volumes displaced in water (Archimedes Principle). The void space (vesicularity) was then calculated from the density difference between the pumiceous sample and the

Table 2
XRF analyses of whole-rock and groundmass samples from the Okataina volcanic centre

Sample no.:	18		18d	
Location:	Tarawera Dome Complex		Tarawera Dome Complex	
	groundmass	whole rock	groundmass	whole rock
SiO_2	75.8	76.55	75.2	75.63
TiO_2	0.18	0.2	0.15	0.21
Al_2O_3	12.94	12.86	13.22	12.76
Fe_2O_3	1.45	1.49	1.35	1.54
MnO	0.06	0.05	0.06	0.06
MgO	0.28	0.29	0.22	0.3
CaO	0.79	1.23	0.91	1.29
Na_2O	4.23	4.19	4.26	4.18
K_2O	4.01	3.28	3.82	3.17
P_2O_5	0.05	0.04	0.03	0.04
Loss	0.14	0.08	0.99	0.73
Total	99.93	100.26	100.21	99.91
Y		22		22
Rb		101		101
U		2.6		2.5
Th		10.1		11.2
Pb		14		14
Zn		25		31
Cu		2		2
Ni		<1		<1
Nb		8		7
Zr		130		136
Sr		106		110
Cr		<1		<1
Ba		839		837
Sc		5		5
V		6		6
La		22		23
Ce		48		48
Nd		21		20

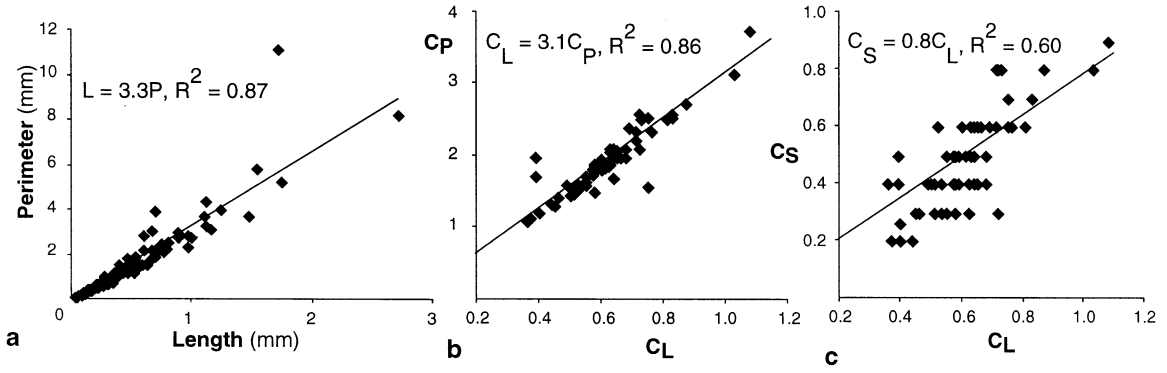

Fig. 1. Two-dimensional image analysis data for feldspar and quartz phenocryst populations. (a) Maximum intersection length versus perimeter for phenocrysts in sample 7. (b) Average maximum intersection length of phenocrysts (C_L in mm) versus the average perimeter of phenocrysts (C_P in mm) in each thin section. (c) Average maximum intersection length of phenocrysts (C_L in mm) versus the standard deviation of phenocryst sizes (sorting; C_S) in each thin section.

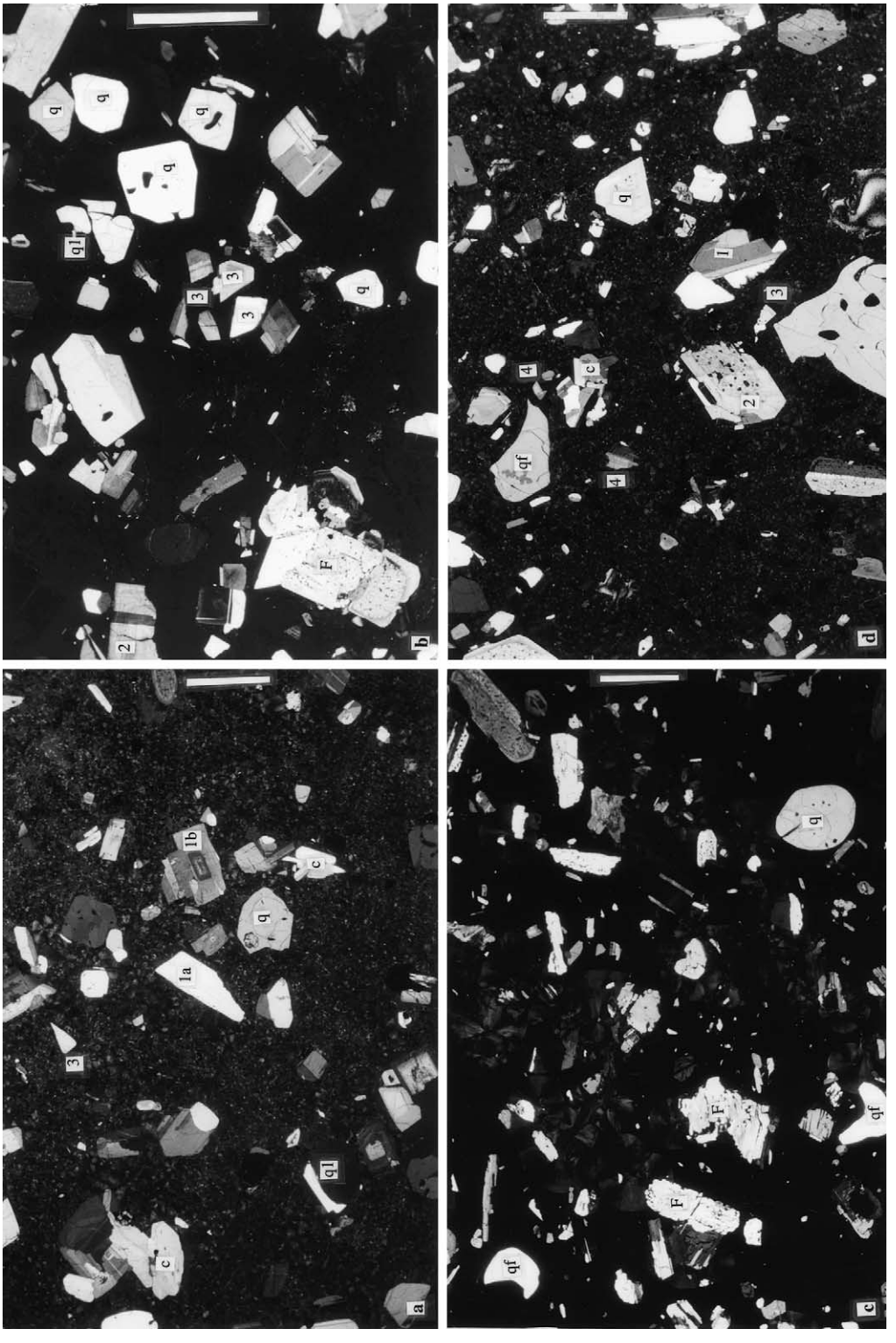
a
1a
1b
c
q
ql
3
b
q
ql
3
F
2
d
q
I
3
4
c
2
qf
4
c
qf
F
F
q
qf

dense sample of the same lava or lava dome (where available). Phenocryst contents were then re-calculated by eliminating the void space (Table 1). For those pumiceous samples without a dense counterpart, 2.25 g/cm^3 was used (average for all dense samples) for the density of the dense rock.

Feldspar and quartz fragments were identified by abrupt changes in zoning, splintery form, curviplanar or ragged outline, or occurrence in clusters with jigsaw-fit texture. Comparisons are made between the total percentage of quartz and feldspar phenocrysts within a sample (A, modal%), the percentage of feldspar and quartz fragments within the sample (F, modal%), and the percentage of the phenocrysts that are fragments (x, %), where $Ax/100 = F$.

3. Shapes of phenocrysts and free crystals

3.1. Feldspar phenocrysts in lavas and lava domes

Feldspar phenocrysts are present both as simply twinned crystals, multiply twinned crystals and as crystal clusters. Most of the feldspars are plagioclase and exhibit polysynthetic twinning, but a small number are simply twinned sanidine. Single feldspar phenocrysts range in length from 0.2–0.8 mm (small) to more than 3.5 mm (large), but most are 0.8–2 mm (medium). Multiply twinned feldspar phenocrysts generally comprise two medium-sized intergrown parts, each of which is polysynthetically twinned, and occur together with several separate, small, tabular, interlocking crystals on the margin. Most crystal clusters comprise three or more intergrown, medium or small, anhedral, polysynthetically twinned crystals.

The feldspar phenocrysts show characteristic oscillatory zoning (Fig. 2a). Both sharply zoned, clear feldspar and mottled, sieve-textured feldspar phenocrysts are present within the same sample (Fig. 2b,d). Both types of feldspar contain relatively large (50 μm) melt inclusions. In addition, cores of the sieve-textured feldspar phenocrysts are riddled with melt inclusions and show diffuse oscillatory zoning. The sieve-textured feldspars are larger than the clear feldspars by a factor of 1.5–2. Although the outer rims of the sieve-textured feldspars are mostly clear and zoned (Fig. 2b), in some cases, the mottled sieve texture continues to the outer margins, creating an irregular outline (Fig. 2c).

Simply twinned phenocrysts generally have exterior faces that are euhedral. Multiply twinned phenocrysts are also euhedral except for the parts intergrown with small, tabular crystals at the margins. The composition planes of the simply twinned phenocrysts and medium intergrown parts of the multiply twinned phenocrysts have abruptly terminated oscillatory zoning or are irregular. The medium or large, simply twinned, sieve-textured feldspars, in particular, have irregular composition planes (Fig. 2b).

The exterior margins of crystals in the crystal clusters are regular crystal faces whereas their in-

Fig. 2. Lava and lava dome samples, New Zealand. (a) Proximal sample, IN30, from the Moerangi dome, Kapenga volcanic centre, comprising 19 modal% dominantly medium feldspar and quartz phenocrysts in a massive, devitrified, formerly glassy groundmass. Medium, type 1 feldspar fragments have a partly diagonal and irregular (1a) or jagged (1b) margin. (b) Proximal sample, 19, from the top of the Tarawera Dome Complex, Okataina volcanic centre, comprising 21 modal% phenocrysts that include a medium, clear and large, sieve-textured feldspar (F). Fragments present include: an isolated, medium, type 2 fragment (2), and a group of small, type 3 fragments that have been separated and rotated (3). The thin section has been cut parallel to the elongation direction of sparse vesicles. (c) Distal sample, 12, from the Tarawera Dome Complex, Okataina volcanic centre. The sample comprises 17 modal% phenocrysts of dominantly irregularly shaped, sieve-textured feldspar (F), and round quartz. The groundmass is massive and glassy with some spherulitic zones. A quartz fragment (qf) is present towards the bottom. (d) Distal sample, IN28, from the Moerangi dome, Kapenga volcanic centre, comprising 28 modal% dominantly medium and small feldspar, and medium and large quartz phenocrysts in a massive, devitrified, formerly glassy groundmass. Fragments present include: chunky, type 2 fragment (2) with an irregular broken margin; type 3 fragment (3) separated and rotated from type 1? (1); anhedral, type 4 fragment (4) separated and rotated from a crystal cluster of anhedral feldspar; quartz fragment (qf) with a sharp, concave broken surface. q1, not a genuine fragment but the remains of a larger crystal partly plucked out during thin-section preparation. c, crystal cluster; q, internally fractured and embayed quartz phenocryst. Crossed nicols. Scale bars, 2 mm.

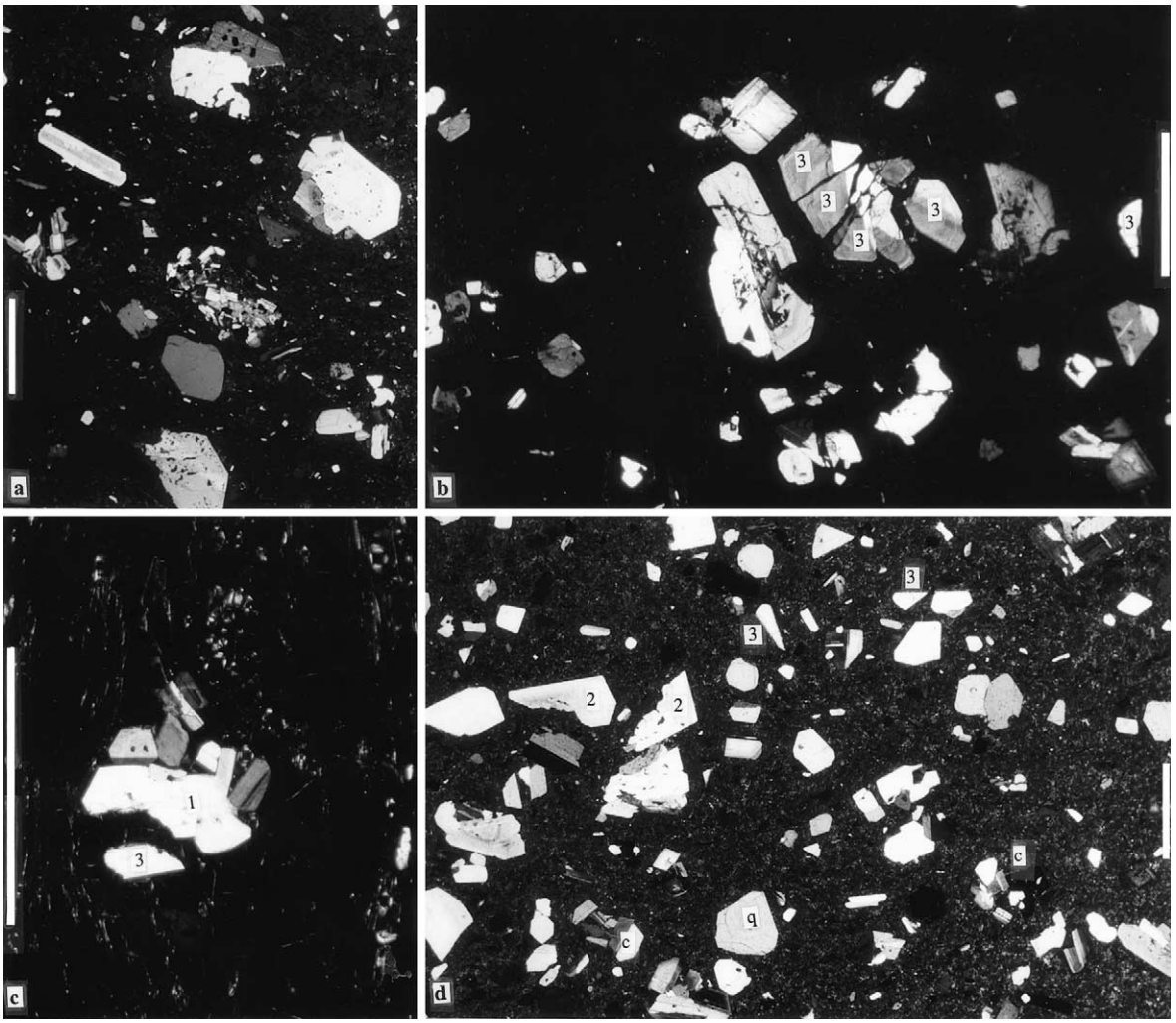

Fig. 3. Lava and lava dome samples, New Zealand. (a) Distal sample, IN24, from the Kapenga volcanic centre, comprising 16 modal%, large and small feldspar and quartz phenocrysts in a finely vesicular groundmass. The fine crystal cluster near the centre has partly disintegrated along the weakly developed flow banding. (b) Distal sample, IN28, from the Moerangi dome, Kapenga volcanic centre, comprising 28 modal% phenocrysts in a massive, devitrified, formerly glassy groundmass. Chunky type 3 feldspar fragments (3) are separated by only a thin selvage of groundmass and remain in a jigsaw-fit arrangement. (c) Close-up of distal sample, 6b, from the Haroharo Dome Complex, Okataina volcanic centre. Types 1 (1) and 3 (3) fragments are separated in the direction of vesicle elongation. (d) Proximal sample, 19b, from the top of the Tarawera Dome Complex, Okataina volcanic centre. The sample contains 20 modal%, dominantly medium and small feldspar and quartz phenocrysts in massive, cryptocrystalline groundmass. There are two, type 2 fragments (2) with irregular broken margins that have been separated and rotated from each other, and two, type 3 fragments (3). Crossed nicols. c, crystal cluster; q, internally fractured quartz phenocryst. Scale bars, 2 mm.

terior margins have irregular (intergrown) outlines and zoning that is abruptly terminated (Fig. 2d). Crystals completely within the clusters are dominantly anhedral. However, some clusters are glomeroporphyritic aggregates and consist of small, tabular plagioclase together with hornblende (Fig. 3a).

Five types of feldspar phenocryst fragments have been identified (Fig. 4). Several types of fragments can occur within one sample. The first type

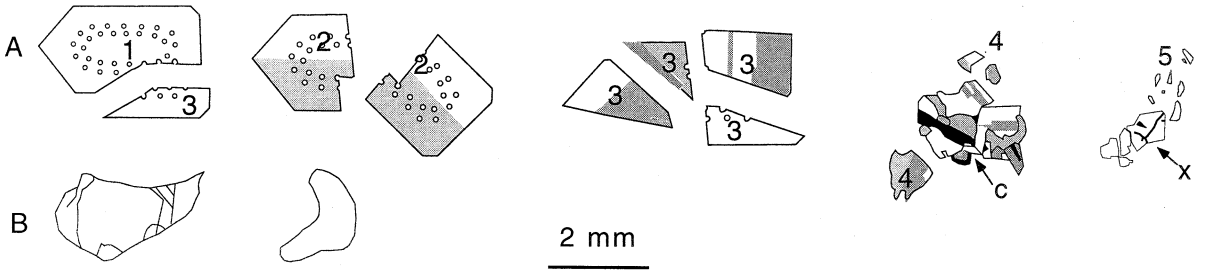

Fig. 4. Line drawing of the five types of phenocryst fragments present in the lava and lava domes samples. (A) Feldspar fragments. Type 1: dominantly euhedral with only a small part that is re-entrant. Type 2: subhedral chunks with broken irregular or straight margins. Type 3: equant or triangular fragment. Type 4: anhedral fragment separated from a crystal cluster (c). Type 5: splinter separated from a strongly fractured phenocryst (x). (B) Dominantly euhedral and subhedral, chunky quartz fragments.

comprises nearly complete, medium or large (>0.8 mm), dominantly euhedral, single untwinned or twinned phenocrysts with only a small part of one face or a corner that is re-entrant (type 1; Figs. 2a,d and 3c). The margin of the broken portion is either jagged or relatively straight but somewhat irregular and dotted with the margins of melt inclusions. The second type of fragment is also medium or large (>0.8 mm) but subhedral. This type mostly occurs as equant (Fig. 2d) or triangular (Fig. 3d) crystal chunks with one main straight but irregular margin. These large and medium, dominantly euhedral and subhedral fragments can be single and isolated (Fig. 2b,d), or else grouped with other fragments from the same parent phenocryst (Fig. 3d).

The third fragment type is small to medium (0.5 mm), equant or triangular, with abruptly terminated oscillatory zoning. Only parts of the original crystal faces are intact and the broken surfaces are either straight, jagged (Figs. 2b and 3b,d) or irregular (Figs. 2a and 3c). These small fragments can be isolated but are commonly grouped (Figs. 2b, 3b and 5a), or are paired (conjugate) with a nearly complete parent phenocryst of type 1 (Fig. 3c). These three types of feldspar fragments are the most common.

The fourth fragment type is small and anhedral. These fragments can be isolated or in groups relatively close to a crystal cluster (Fig. 2d). The final type is small (0.2 mm) and splintery, with sharply angular margins. The splinters are relatively rare (<0.1%) and concentrated within spherulitic or cryptocrystalline groundmass domains. The cryptocrystalline domains are irregularly shaped, elongate, brown in thin section and contained within otherwise glassy groundmass (Fig. 5b). Hence, the cryptocrystalline domains are probably devitrified. The splinters also occur close to intensely fractured phenocrysts.

In some cases, the grouped or conjugate fragments are separated by only a thin selvage of the glassy (or formerly glassy) groundmass and remain in a jigsaw-fit arrangement (Fig. 3b,c). In other cases, the fragments are more widely separated (>50 μm) by groundmass and are rotated (Figs. 2b,d and 3d). In tube pumice samples, conjugate fragments are aligned parallel to the vesicle elongation direction (Fig. 3c). In samples with massive, glassy or crystalline groundmass, the conjugate fragments are not aligned (Fig. 3d). Within some flow bands, small tabular crystals occur close to glomeroporphyritic aggregates composed of similar small tabular crystals (Fig. 3a).

3.2. Quartz phenocrysts in lavas and lava domes

Most samples contain quartz phenocrysts. These phenocrysts are medium to large (1.5–3.5 mm) and internally fractured. They include large melt inclusions (up to 0.2 mm) and are slightly to strongly embayed (Figs. 2b–d, 3d and 5a). In some samples, euhedral prismatic quartz phenocrysts are present (Figs. 2b and 3d). However, in most cases, the quartz phenocrysts are round (Figs. 2c and 5a). Fracture surfaces are mostly conchoidal (Figs. 2a,c), but some are irregular

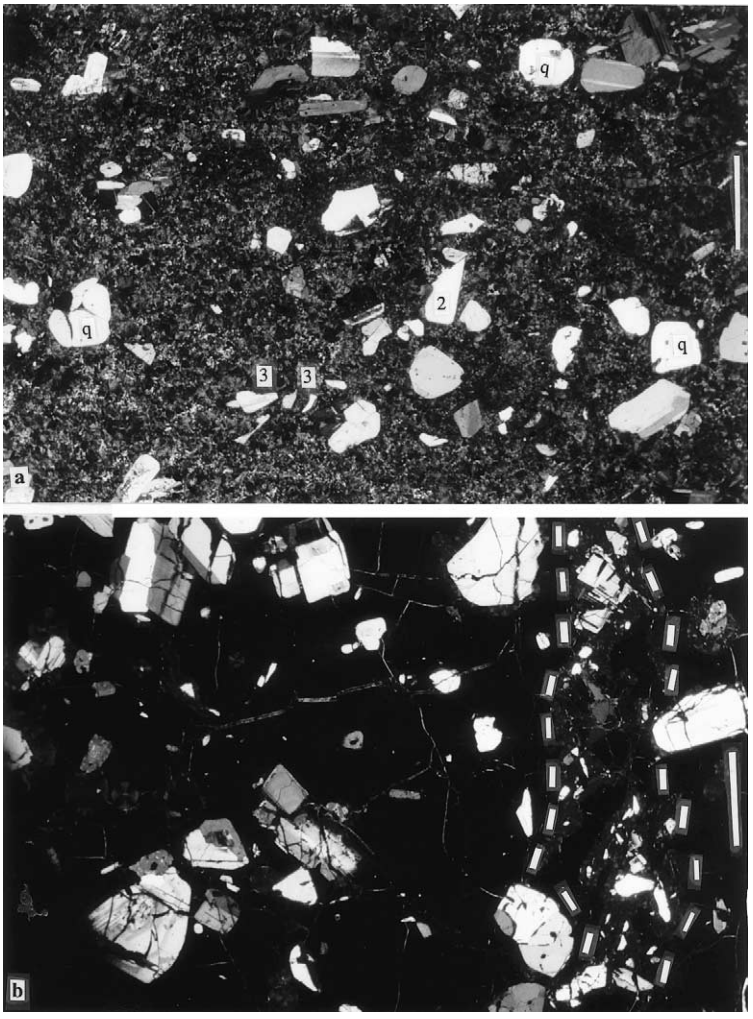

Fig. 5. Lava and lava dome samples, New Zealand. (a) Distal sample, IN11, from the Tutakeheke dome, Kapenga volcanic centre. The sample contains 16 modal%, medium feldspar and quartz phenocrysts within a devitrified, formerly glassy groundmass. Small type 3 fragments (3) occur in a group separated by groundmass. A quartz phenocryst (q) shows a deep embayment along conchoidal fractures. (b) Distal sample, 13, from the Kapenga volcanic centre, comprising 19 modal%, dominantly large feldspar phenocrysts in a mainly massive, glassy groundmass. Phenocryst splinters (circled area) are concentrated in a devitrified zone on the right-hand side of the photo. Both the groundmass and phenocrysts show brittle fractures. Crossed nicols. Scale bars, 2 mm.

(Fig. 2d) and intersect melt inclusions or embayments. In some cases, thin selvages of groundmass occur along the conchoidal fractures, creating a cluster of subround quartz beads (Fig. 5a).

Quartz fragments are also present. In comparison to the feldspar fragments, all the quartz fragments are angular and have sharply defined margins, which are either concave or convex (Fig. 4). Many quartz fragments are parts of relatively equant (or round) crystals (Fig. 2c,d). In addition, the quartz fragments are typically solitary rather than conjugate pairs.

3.3. *Phenocrysts in block and ash flow clasts*

Feldspar and quartz phenocrysts in juvenile clasts from the Kaharoa block and ash flow deposits are similar to those found within the lava

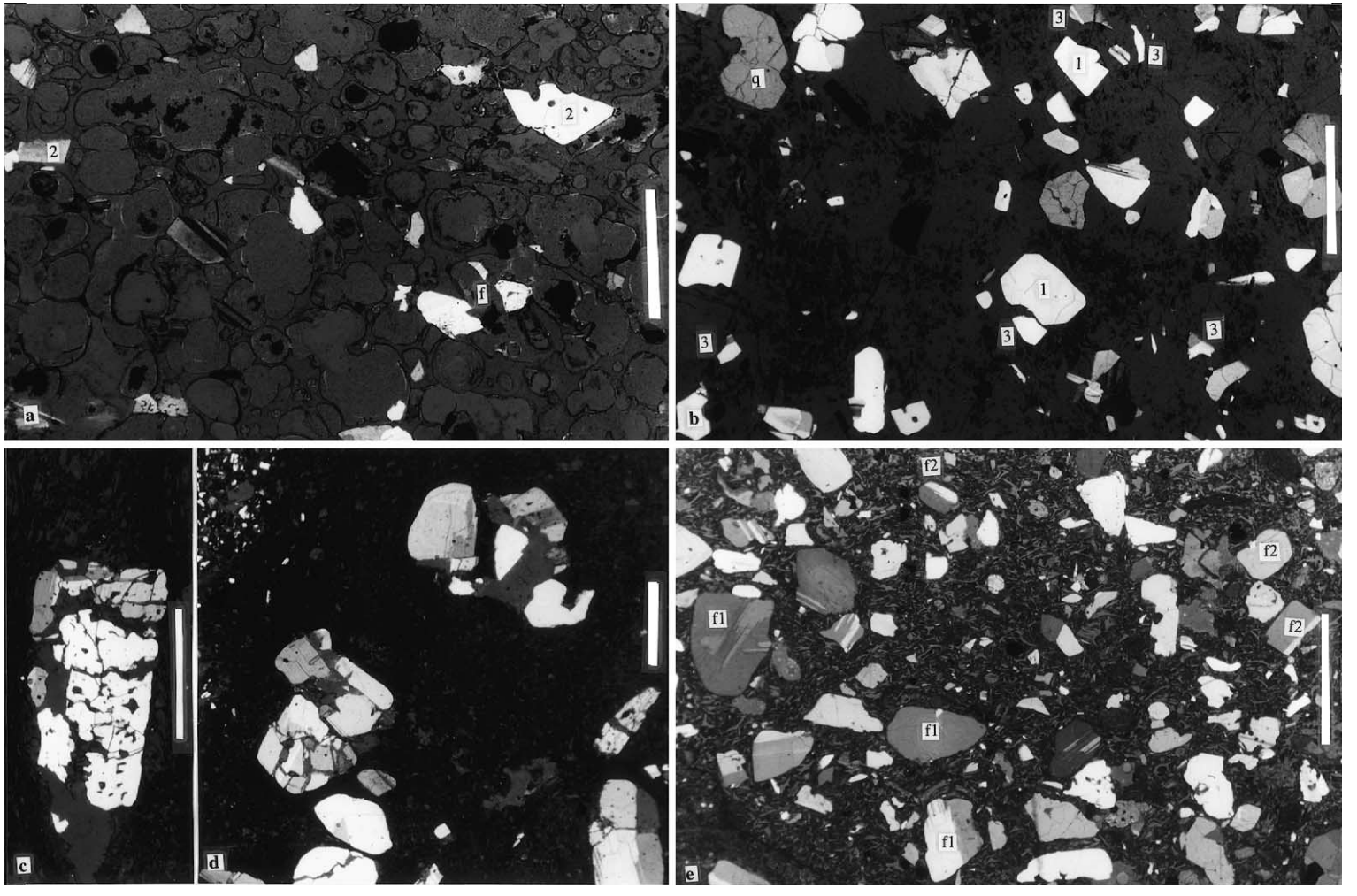

Fig. 6. (a,b) Block and ash flow clasts, Kaharoa eruptive episode, Okataina volcanic centre, New Zealand. (c–e) Ongatiti Ignimbrite, Mangakino volcanic centre, New Zealand. (a) Sample K1 comprises at least two type 2 fragments (2) in a moderately vesicular groundmass. Feldspar fragments, f, are the remnants of larger crystals partly plucked out during thin-section preparation. (b) Sample K1d has a non-vesicular glassy groundmass with perlitic cracks. Several type 3 fragments (3) are present one of which can be fitted with a type 1 fragment (1). Embayed and fractured quartz phenocryst (q). (c) Pumice sample, A12p1, with intensely fractured, sieve-textured feldspar phenocryst, equivalent to type 3 fragments. (d) Pumice sample A12p1. Intensely fractured phenocrysts equivalent to equant and splintery type 3 and 5 fragments. (e) Crystals within the ignimbrite matrix show a wide range of size and shape. Most are anhedral fragments with some sub-rounded feldspar (f1) and nearly complete euhedral feldspar (f2). Crossed nicols. Scale bar, 2 mm.

and lava dome samples. Both simply twinned and multiply twinned feldspar phenocrysts are present, as are internally fractured quartz phenocrysts (Fig. 6a,b). Feldspar fragments are dominantly medium and large, euhedral and subhedral fragments (types 1 and 2) and small, equant or triangular fragments (type 3). Quartz fragments are subhedral and have at least one irregular face.

3.4. Crystals in ignimbrite

Phenocrysts within pumice clasts of the Ongatiti Ignimbrite are noticeably different from those in the lava, lava dome and block and ash flow samples. The feldspar and quartz phenocrysts are intensely fractured and fragments are separated by void spaces that range from a few microns to hundreds of microns across (Fig. 6c,d). Within sieve-textured feldspar, the fractures cut through large melt inclusions and fracture surfaces have smoothly irregular shapes (Fig. 6c). Less intensely fractured feldspar and quartz phenocrysts are cut by sharp and jagged fractures, producing fragments that range from chunky types 1 and 2, to more triangular and splintery types 3 and 5.

Crystals within the matrix of the ignimbrite are dominantly fragments that show a wide range in size (from large to small) and shape, from partly euhedral to anhedral, and from subrounded to equant (Fig. 6e).

3.5. Pyroxene phenocrysts

Although not studied in detail, pyroxene phenocrysts are apparently much less prone to fracturing than quartz and feldspar phenocrysts in all samples (lavas, lava domes, block and ash flow clasts, ignimbrite pumice). These phenocrysts are mostly euhedral.

4. Abundances of phenocrysts and phenocryst fragment populations

The abundance of quartz and feldspar phenocrysts in the lava and lava dome samples ranges between 1 and 28 modal%. Nearly all the lava and lava dome samples include phenocryst fragments; the average abundance of fragments (x) is 5% of the total phenocryst population, with a maximum of 19% (x), corresponding to 2.4 modal% (F). Very few ($<10\%$) samples contain more than 12% fragments in the total phenocryst population. The abundance of phenocryst fragments shows considerable scatter (Fig. 7a,b) and relatively weak multiple regression correlation coefficients (R^2). However, least-squares regression lines for pumiceous (recalculated) and dense lava and lava dome samples are similar and the modal% of phenocryst fragments (Fr) approximates $0.04A$, or for x, $xr = -0.24A + 8.4$ (Fig. 7a). The maximum value for F, Fmax, is $0.19A$ (Fig. 7a). Hence, lavas and lava domes with low phenocryst contents contain few fragments (0.3 modal% for samples with less than 4 modal% phenocrysts; Fig. 7a), whereas those with higher phenocryst contents have more fragments (0.8 modal% for samples with 20 modal% phenocrysts).

Although the modal percentage of phenocryst fragments (F) in lavas and lava domes with low phenocryst contents is relatively small, the proportion of phenocryst fragments in the crystal population, x, is highly variable (Fig. 7b): for total phenocryst contents up to 10 modal %, the proportion of fragments (x) ranges from 0.2% to 19% (i.e. for $A \leq 10\%$: $0.2\% < x < 19\%$). Hence, the presence of only one or a few fragments in samples with low phenocryst contents strongly affects x.

The abundance of phenocryst fragments in the block and ash flow clasts is similar to that within lavas and lava domes, although at the higher end of the range, particularly for the breadcrusted vesicular samples (Fig. 7a,b). The ignimbrite pumice and matrix samples have a similar range of phenocryst modal abundance (8–25%) to the lava and lava dome samples (1–28%). However, there are significant differences between the abundances of phenocryst fragments in lava and lava domes compared to the ignimbrite sample (Fig. 7c,d). Phenocryst fragments in the ignimbrite pumice and crystal fragments in the ignimbrite matrix comprise more than 67% of the total crystal population (cf. $<19\%$ for lava and lava domes).

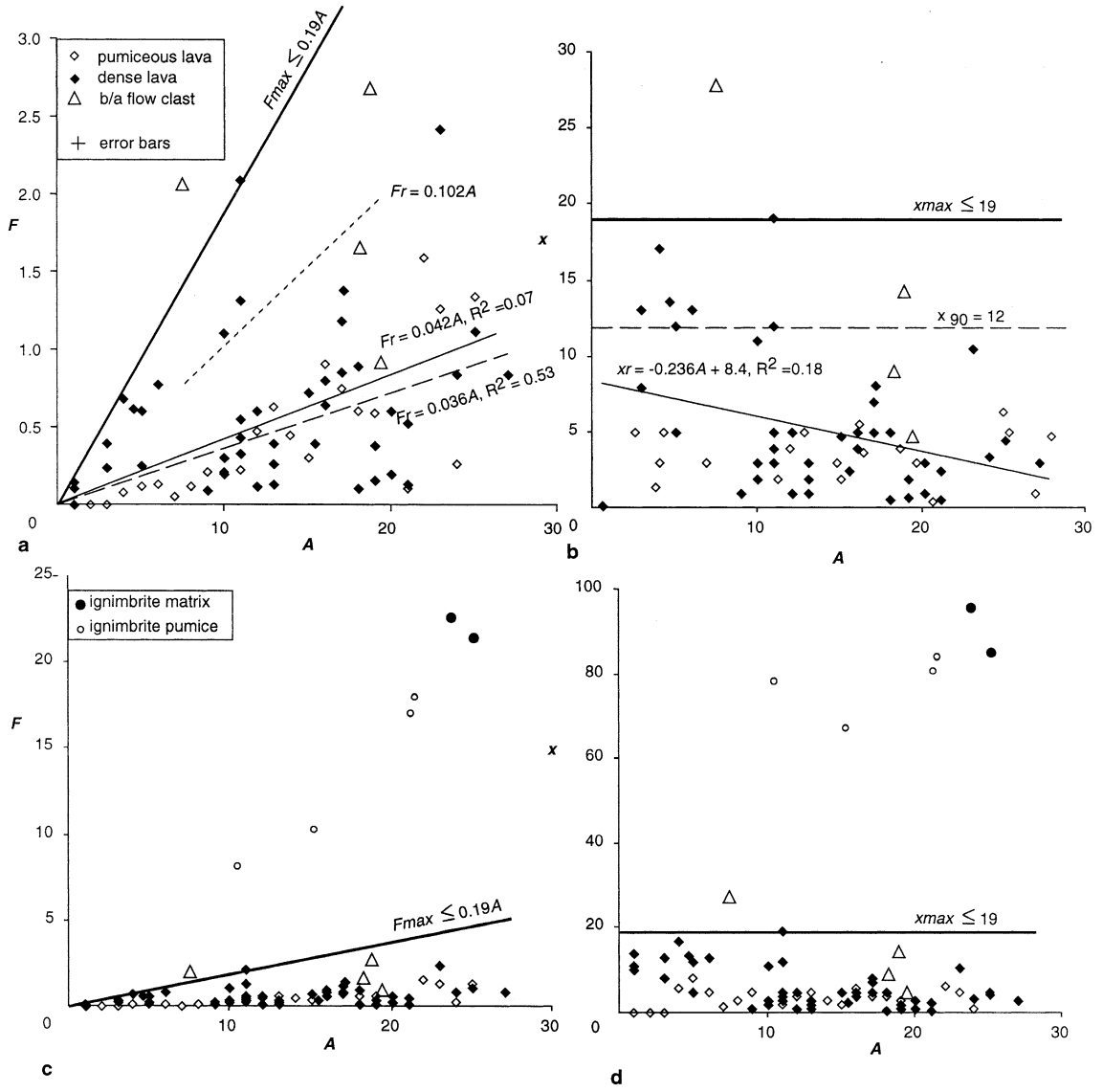

Fig. 7. Modal% quartz and feldspar phenocrysts (A) versus the abundance of phenocryst fragments and crystal fragments. (a,c) Modal% phenocryst fragments (F). (b,d) Percentage of crystal fragments in the crystal population (x). (a) Lava and lava dome samples (diamonds) and block and ash flow clasts (triangles). Heavy solid line, estimation of Fmax. Linear regression trends (Fr): short dash – block and ash flow clasts (Fr = 0.102A), solid line – dense lava and lava dome samples (Fr = 0.042A), long dash – pumiceous lava and lava dome samples (Fr = 0.036A). (b) Lava and lava dome samples (diamonds) and block and ash flow clasts (triangles). Heavy solid line – $x$max. Negative linear regression trend for lava and dome samples – solid line (xr = −0.236A+8.4). (c,d) Lava and lava dome samples (diamonds) and block and ash flow clasts (triangles) compared with ignimbrite pumice (open circles) and matrix (filled circles). Ignimbrite matrix has the highest percentage of crystal fragments. Ignimbrite pumice plots well above the maximum values for fragments in lavas and lava domes.

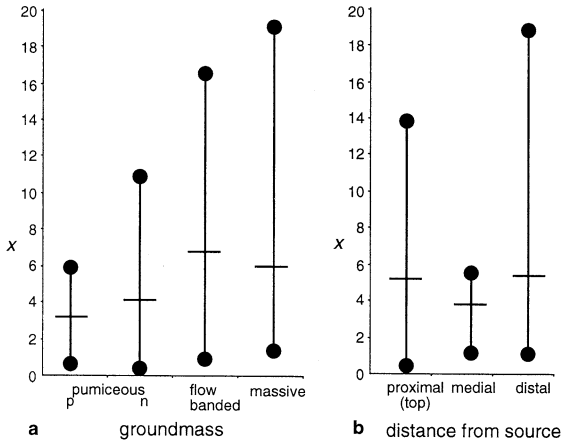

Fig. 8. Maximum, minimum and average values for phenocryst fragments in lavas and lava domes. (a) The average of the proportion of fragments in the phenocryst population (x) is not obviously correlated with various groundmass textures. p, parallel to vesicle elongation; n, normal to vesicle elongation. (b) The average of the percentage of fragments in the phenocryst population (x) shows no significant correlation with distance from source.

The percentage of fragments in the total phenocryst population (x) of the lavas and lava domes appears unrelated to the groundmass texture and is similar in pumiceous and non-vesicular, glassy and crystalline, massive and flow-banded groundmasses (Fig. 8a). The percentage of fragments in the total phenocryst population (x) for samples from the distal parts of the lavas or lava domes is only slightly higher than that of samples from close to the vent (proximal) or from the middle (medial) (Fig. 8b). Thus, there is no clear correlation between the proportion of phenocryst fragments and either groundmass texture or distance from source in the rhyolitic lavas and lava domes sampled.

5. Discussion

5.1. Origins of the phenocrysts

The crystal clusters, embayed quartz, large sieve-textured feldspar and clear feldspar indicate mixed origins for the phenocrysts in the rhyolitic lavas and lava domes sampled. The clear, euhedral feldspars with regular oscillatory zoning were probably in equilibrium with the melt, and hence, intratelluric. The small and medium feldspars in the crystal clusters are also clear and subhedral to anhedral, suggesting that they too are intratelluric. The large, sieve-textured feldspar phenocrysts, however, have a more complex history, and many of the quartz phenocrysts have embayed external margins that indicate resorption. Nevertheless, these phenocrysts also appear to have crystallised from melt and to have been suspended in melt, though not necessarily the melt represented by the presently surrounding groundmass. Hence, we infer that any fragmentation of the crystals occurred during magma withdrawal, eruption and/or outflow.

5.2. Origins of phenocryst fragments in lavas and lava domes

Although there are five types of feldspar fragments, most occur in pairs or groups derived from a single, complete parent phenocryst. At least half of the feldspar fragments are nearly complete, medium or large, single, untwinned or twinned, dominantly euhedral phenocrysts with only a small part of one face or corner that is re-entrant (type 1). In many cases, a conjugate, small to medium, generally equant or triangular fragment (type 3) resides in close proximity to a larger type 1 fragment. These fragments fit together as in a jigsaw puzzle. Similarly, the subhedral (type 2) crystal chunks commonly occur together in conjugate pairs, and the splintery (type 5), and anhedral (type 4) fragments also occur in groups. These conjugate paired and grouped fragments form either jigsaw-fit, or clast-rotated arrangements. Some are separated by groundmass domains up to three times the size of the fragment. Hence, some of the apparently isolated fragments may also be part of a conjugate pair or a jigsaw-fit group, but the matching part(s) lies outside the area sampled by the thin section. Hence, most fragments were probably derived from nearby, single, larger parent phenocryst or crystal clusters. The isolated quartz fragments are exceptional in their lack of association with an obvious nearby parent phenocryst.

Many of the phenocryst fragments appear to have broken along zones of internal weakness. For example, many quartz fragments have a broken margin that is concave and that can be matched with internal conchoidal fractures or interconnecting embayments. Similarly, the anhedral feldspar fragments (type 4) appear to have been anhedral crystals in crystal clusters that separated along the intergrown internal faces. In addition, the separation of some of the small fragments (type 3) from nearly whole phenocrysts, and of the crystal chunks (type 2), appears to have occurred either along the composition planes of twinned phenocrysts, or where the margin is jagged, along cleavage planes. Some small phenocrysts concentrated within flow bands are derived from disintegration of fine-grained crystal aggregates nearby.

Small fragments and chunks with very irregular broken margins may have separated from feldspar phenocrysts with large melt inclusions or from sieve-textured feldspars, and many of the fractures within the quartz phenocrysts are centred on melt inclusions, suggesting that inclusions were relatively weak and promoted internal failure. Melt inclusions will contribute to cracking of the host phenocryst during magma ascent because they have relatively large elastic moduli and produce local stress that can exceed the tensile strength of the phenocryst (Tait, 1992). Vesiculation within the melt inclusion during decompression will result in large increases in internal pressure, causing the host crystal to fracture, a mechanism also thought to cause crystal fracture in explosive eruptions (e.g. Best and Christiansen, 1997). The sieve-textured feldspar and quartz phenocrysts are the most prone to fracturing by this process as they contain multiple or large inclusions, which, in the case of the sieve-textured feldspars, are separated by relatively thin walls (cf. Tait, 1992). In addition, separation of fragments from the quartz phenocrysts may have resulted from interconnection of deeply penetrating embayments.

As many of the phenocryst fragments are separated by groundmass or have been rotated, fragmentation must have occurred while the melt phase was still molten and moving, during withdrawal, eruption and/or outflow. However, the close proximity of many of the feldspar fragments to their parent phenocryst, and the overall even distribution of phenocrysts and phenocryst fragments, suggest that separation occurred relatively late in the outflow, but while the lava flows were still ductile. Most of the quartz fragments are isolated and not related to jigsaw-fit groups. Hence, fragmentation of the quartz phenocrysts may have begun earlier than fragmentation of the feldspars, allowing greater separation of the fragments.

The lavas and lava domes display flow banding, flow folds, distortion of foliations around rotated solid bodies, and lineations on foliation or flow-band surfaces, all of which indicate that flow involved laminar shear. With continuing laminar shear, prepared fractures in the phenocrysts will progressively open and dilate, causing the fragments to separate and rotate from the parent phenocryst. Laminar shear may also be an important in causing disintegration of crystal aggregates. Many aggregates have disintegrated, generating type 4 fragments, and the fragments are strung out in flow bands. In this case, single crystals within the aggregates may have separated along the structurally weak boundaries between the crystals.

5.3. *Phenocryst splinters in lavas and lava domes*

The phenocryst splinters are small, sharply angular and occur in groups close to an intensely fractured phenocryst. The parent phenocryst appears to have disintegrated in a brittle fashion, regardless of any zones of weakness. Similar splintery phenocryst fragments have been found in the Ngongotaha lava dome, New Zealand (Dadd, 1992), and the Badlands rhyolite, USA (Manley, 1996b). In the Badlands rhyolite, phenocryst splinters, bubble-wall shards, and fragments of pumice and dense glass are commonly present in flow bands within the upper obsidian. Manley (1996b) concluded that debris generated by intense comminution of solid lava filled open spaces which were then closed, annealed, and distorted further during continued flow. In the Ngongotaha lava dome, Dadd (1992) found that phenocryst

splinters were concentrated at the boundary between breccia and coherent flow-banded rhyolite.

We propose a similar origin for phenocryst splinters in the lava and lava dome samples studied. The phenocryst splinters are most abundant within devitrified, formerly glassy domains in otherwise glassy but fractured groundmass (e.g. Fig. 5b). The devitrified zones appear to be marking the traces of brittle fractures that initially formed in near-solid glass, perhaps in response to cooling contraction, extension, shear or a combination. Phenocryst splinters generated by propagating fractures would have collected in the cracks. The splinters would have been trapped if the cracks closed and the glass annealed. Glass lining the fractures has preferentially devitrified, perhaps because of hydration on exposure to the atmosphere and/or steam-rich volcanic gas while still open. Devitrification is significantly faster in hydrated glasses than in non-hydrated (Lofgren, 1970).

5.4. Comparison with crystal fragments in ignimbrite

Most of the rhyolitic lavas and lava domes we sampled have less than 19% of their phenocryst population as fragments. In addition, the phenocryst fragments in the lava and lava dome samples are dominantly large (up to 3.5 mm) parts of euhedral parent phenocrysts with only a small part missing (type 1), medium (0.8–2 mm), subhedral, equant chunks (type 2), and small to medium (0.5 mm), equant or triangular fragments (type 3). Phenocryst splinters are volumetrically minor ($<0.1\%$). In comparison, most crystals in ignimbrites are fragments (e.g. 67–96% of the crystal population in the Ongatiti ignimbrite). In addition, the fragment types in ignimbrites differ from those in lavas and lava domes. Phenocrysts in the ignimbrite pumice are intensely fractured into numerous small type 3 and type 5 fragments and very few of the larger type 1 and type 2 fragments, similar to the 'phenoclasts' found by Best and Christiansen (1997). Ross and Smith (1961) also noted that many of the crystals in ignimbrites had sharply angular outlines, and most crystal faces were cut by irregular fracture surfaces, similar to the phenocryst splinters. A greater number of larger type 1 and 2 fragments are found in the ignimbrite matrix where the crystals are more concentrated, however, these fragments are generally subrounded.

Crystal breakage in ignimbrites has been attributed to rapid decompression during explosive eruption and impact during eruption and transport within a pyroclastic flow (Fisher and Schmincke, 1984). Best and Christiansen (1997) considered the latter process to be less important than rupture in response to expansion of gas bubbles within melt inclusions during syn-eruptive decompression. Juvenile pumice clasts and matrix of the ash-flow tuffs they studied include plagioclase fragments that are bordered by melt inclusions and commonly occur in jigsaw-fit groups (Best and Christiansen, 1997). Rapid decompression generated multiple fragments from one parent crystal. Decompression rates for effusive eruptions of rhyolitic lava are significantly lower than those for explosive eruptions, allowing passive, non-explosive degassing accompanied by slower ascent rates (Gardner et al., 1999). In the lavas and lava domes, parent phenocrysts are generally separated into only two parts, even where the surrounding groundmass is pumiceous, perhaps reflecting the slower ascent rate that allowed 'leaky' behaviour of phenocrysts with melt inclusions.

6. Conclusions

Most porphyritic small-volume, rhyolitic lavas and lava domes with relatively high viscosities (in the range of 10^{10}–10^{11} Pa s) include a population of phenocryst fragments. The percentage of feldspar and quartz fragments in the total phenocryst population for these lavas and lava domes is around 5%. In addition, the maximum percentage of feldspar and quartz fragments in the phenocryst population rarely exceeds 12%, even in lavas with high phenocryst contents (up to 28 modal%). Hence, the modal abundance of phenocryst fragments in lavas and lava domes is small, generally 0.5 modal% with a maximum of 2 modal%. The percentage of phenocryst fragments shows no

clear correlation with distance from source nor with groundmass texture (whether non-vesicular or vesicular glass, or crystalline, flow-banded rhyolite).

The rhyolitic lavas and lava domes include sieve-textured and clear, simply and multiply twinned feldspar, single quartz phenocrysts and feldspar crystal clusters. The phenocryst fragments are dominantly medium to large (>0.5 mm), and derived from euhedral crystals from which only a small part has been removed, or are subhedral with only one irregular margin, or anhedral and equant. Most of the phenocryst fragments occur in conjugate pairs or groups that together form a complete crystal. In many cases, a small to medium fragment resides in a jigsaw-fit or clast-rotated arrangement near the medium or large parent fragment. Many of the phenocryst fragments appear to have broken along zones of internal weakness. Quartz fragments have separated along embayments and conchoidal fractures. Feldspar phenocrysts have broken along structural weaknesses such as zones of melt inclusions, cleavage surfaces and composition planes of twins. Some anhedral feldspar fragments are derived from disintegration of crystal clusters composed of anhedral crystals. Separation and rotation of the fragments occurred in response to shear during laminar flow. With continuing shear, the fractures progressively opened and fragments separated. Fractures may have formed in response to decompression during magma ascent, especially in phenocrysts with abundant and/or large melt inclusions. Small phenocryst splinters (<0.2 mm) are relatively rare ($\ll 0.1\%$) and are attributed to comminution of near-solid parts of lavas and lava domes.

In comparison with ignimbrites, rhyolitic lavas and lava domes contain significantly fewer phenocryst fragments. Phenocryst fragments generally occur in jigsaw-fit or clast-rotated pairs or groups, and the proportion phenocryst splinters is only minor ($<0.1\%$). In ancient deformed, altered and/or poorly exposed silicic volcanic successions, data on crystal fragment abundance and shape can assist distinction of lava and lava dome facies from pyroclastic facies.

Acknowledgements

This research was funded by the Australian Research Council through the Special Research Centres programme and by a Postdoctoral Fellowship held by S.A. Critical reviews of an earlier manuscript by Michael Higgins, Kathy Cashman and Bruce Marsh are greatly appreciated. This paper also benefited from discussions with Vadim Kamenetsky. The authors wish to thank Ian Nairn for help with selecting suitable sample sites, logistical advice and providing samples from the Kapenga volcanic centre. J.McP received support from the Institute of Geological and Nuclear Sciences, Wairakei Research Centre, during manuscript preparation. XRF analyses were performed at the University of Tasmania by Analyst, P. Robinson.

References

Allen, R., 1988. False pyroclastic textures in altered silicic lavas, with implications for volcanic-associated mineralization. Econ. Geol. 83, 1424–1446.

Allen, S.R., 2001. Reconstruction of a major caldera-forming eruption from pyroclastic deposit characteristics: Kos Plateau Tuff, eastern Aegean Sea. J. Volcanol. Geotherm. Res. 105, 141–162.

Allen, S.R., McPhie, J., 2002. The Eucarro Rhyolite, Gawler Range Volcanics, South Australia: A >675 km^3 compositionally zoned lava of Mesoproterozoic age. Geol. Soc. Am. Bull. 114, 1592–1609.

Best, M.G., Christiansen, E.H., 1997. Origin of broken phenocrysts in ash-flow tuffs. Geol. Soc. Am. Bull. 109, 63–73.

Bonnichsen, B., Kauffman, D.F., 1987. Physical features of rhyolite lava flows in the Snake River Plain volcanic province, southwestern Idaho. In: Fink, J.H. (Ed.), The Emplacement of Silicic Domes and Lava Flows. Geol. Soc. Am. Spec. Pap. 212, 119–145.

Branney, M.J., Kokelaar, B.P., McConnell, B.J., 1992. The Bad Step Tuff: a lava-like rheomorphic ignimbrite in a calc-alkaline piecemeal caldera, English Lake District. Bull. Volcanol. 54, 187–199.

Burt, R.M., Cole, J.W., Vroon, P.Z., 1996. Volcanic geology and geochemistry of Motuhora (Whale Island), Bay of Plenty, New Zealand. N.Z. J. Geol. Geophys. 39, 565–580.

Christiansen, R.L., Lipman, P.W., 1966. Emplacement and thermal history of a rhyolite lava flow near Fortymile Canyon, Southern Nevada. Geol. Soc. Am. Bull. 77, 671–684.

Cole, J.W., Thordarson, T., Burt, R.M., 2000. Magma origin and evolution of White Island (Whakarri) volcano, Bay of Plenty, New Zealand. J. Petrol. 41, 867–895.

Dadd, K.A., 1992. Structures within large volume rhyolite lava flows of the Devonian Comerong Volcanics, southeastern Australia, and the Pleistocene Ngongotaha lava dome, New Zealand. J. Volcanol. Geotherm. Res. 54, 33–51.

Eichelberger, J.C., Chertkoff, D.G., Dreher, S.T., Nye, C.J., 2000. Magmas in collision: Rethinking chemical zonation in silicic magmas. Geology 28, 603–606.

Eichelberger, J.C., Lysne, P.C., Miller, C.D., Younker, L.W., 1985. Research drilling at Inyo domes, California: 1984 results. EOS Trans. AGU 66, 186–187.

Ewart, A., 1968. The petrography of the central North Island rhyolitic lavas. Part 2 - Regional petrography including notes on associated ash flow pumice deposits. N.Z. J. Geol. Geophys. 11, 478–545.

Ewart, A., Healy, J., 1965. Rotorua-volcanic geology. In: Thompson, B.N., Kermode L.O., Ewart, A. (Eds.), New Zealand Volcanology, Central Volcanic Region. Dept. Sci. Indus. Res. Inform. Ser. 50, 10–26.

Ewart, A., Green, D.C., Carmichael, I.S.E., Brown, F.H., 1971. Voluminous low temperature rhyolitic magmas in New Zealand. Contrib. Mineral. Petrol. 33, 128–144.

Ewart, A., Hildreth, W., Carmichael, I.S.E., 1975. Quaternary acid magma in New Zealand. Contrib. Mineral. Petrol. 51, 1–27.

Fink, J.H., 1983. Structure and emplacement of a rhyolite obsidian flow: Little Glass Mountain, Medicine Lake Highland, northern California. Geol. Soc. Am. Bull. 94, 362–380.

Fink, J.H., Manley, C.R., 1987. The origin of pumiceous and glassy textures in rhyolite flows and domes. In: Fink, J.H. (Ed.), The Emplacement of Silicic Domes and Lava Flows. Geol. Soc. Am. Spec. Pap. 212, 77–88.

Fisher, R.V., Schmincke, H.-U., 1984. Pyroclastic rocks. Springer, New York, 472 pp.

Francalanci, L., Varekamp, J.C., Vougioukalakis, G., Defant, M.J., Innocenti, F., Manetti, P., 1995. Crystal retention, fractionation and crystal assimilation in a convecting magma chamber, Nisyros Volcano, Greece. Bull. Volcanol. 56, 601–620.

Fytikas, M., Innocenti, F., Kolios, N., Manetti, P., Mazzuoli, R., Poli, G., Rita, F., Villari, L., 1986. Volcanology and petrology of volcanic products from the island of Milos and neighbouring islets. J. Volcanol. Geotherm. Res. 28, 297–317.

Gamble, J.A., Wood, C.P., Price, R.C., Smith, I.E.M., Stewart, R.B., Waight, T., 1999. A fifty year perspective of magmatic evolution on Ruapehu Volcano, New Zealand: verification of open system behavious in an arc volcano. Earth Planet. Sci. Lett. 170, 301–314.

Gardner, J.E., Hilton, M., Carroll, M.R., 1999. Experimental constraints on degassing of magma: isothermal bubble growth during continuous decompression from high pressure. Earth Planet. Sci. Lett. 168, 201–218.

Garner, A., McPhie, J., 1999. Partially melted lithic megablocks in the Yardea Dacite, Gawler Range Volcanics, Australia: implications for eruption and emplacement mechanisms. Bull. Volcanol. 61, 396–410.

Gibson, R.G., Naney, M.T., 1992. Textural development of mixed, finely porphyritic silicic volcanic rocks, Inyo Domes, eastern California. J. Geophys. Res. 97, 4541–4559.

Harford, C.L., Sparks, R.S.J., 2001. Recent remobilisation of shallow-level intrusions on Montserrat revealed by hydrogen isotope composition of amphiboles. Earth Planet. Sci. Lett. 185, 285–297.

Henry, C.D., Price, J.G., Rubin, J.N., Parker, D.F., Wolff, J.A., Self, S., Franklin, R., Barker, D.S., 1988. Widespread, lavalike silicic volcanic rocks of Trans-Pecos, Texas. Geology 16, 509–512.

Henry, C.D., Price, J.G., Rubin, J.N., Laubach, S.E., 1990. Case study of an extensive silicic lava: the Bracks Rhyolite, Trans-Pecos, Texas. J. Volcanol. Geotherm. Res. 43, 113–132.

Higgins, M.D., 1996. Magma dynamics beneath Kameni volcano, Thera, Greece, as revealed by crystal size and shape measurements. J. Volcanol. Geotherm. Res. 70, 37–48.

Lofgren, G.E., 1970. Experimental devitrification rate of rhyolite glass. Geol. Soc. Am. Bull. 81, 553–560.

Lofgren, G.E., 1971. Experimentally produced devitrification textures in natural rhyolite glass. Geol. Soc. Am. Bull. 82, 111–124.

Manley, C.R., 1992. Extended cooling and viscous flow of large, hot rhyolite lavas: implications of numerical modeling results. J. Volcanol. Geotherm. Res. 53, 27–46.

Manley, C.R., 1996a. Physical volcanology of a voluminous rhyolite lava flow: the Badlands lava, Owyhee Plateau, southwestern Idaho. J. Volcanol. Geotherm. Res. 71, 129–153.

Manley, C.R., 1996b. In situ formation of welded tuff-like textures in the carapace of a voluminous silicic lava flow, Owyhee County, SW Idaho. Bull. Volcanol. 57, 672–686.

Manley, C.R., Fink, J.H., 1987. Internal textures of rhyolite flows as revealed by research drilling. Geology 15, 549–552.

McBirney, A.R., Murase, T., 1984. Rheological properties of magmas. Annu. Rev. Earth Planet. Sci. 12, 337–357.

McKenzie, D.P., 1972. Active tectonics of the Mediterranean region. Geophys. J. R. Astron. Soc. 30, 109–185.

McPhie, J., Doyle, M., Allen, R., 1993. Volcanic Textures. CODES, University of Tasmania, Hobart, 190 pp.

Nairn, I.A., 1981. Some studies of the geology, volcanic history, and geothermal resources of the Okataina volcanic centre, Taupo Volcanic Zone, New Zealand. Ph.D. Thesis, Victoria University, Wellington (unpubl.).

Nairn, I.A., 1989. Sheet V16AC Tarawera; Geological Map of New Zealand 1:50,000. Dept. Sci. Indus. Res., Wellington.

Nairn, I.A., Wood, C.P., 1987. Active volcanoes of the Taupo Volcanic zone. N.Z. Geol. Surv. Rec. 22, 5–84.

Nairn, I.A., Self, S., Cole, J.W., Leonard, G.S., Scutter, C., 2001. Distribution, stratigraphy, and history of proximal deposits from the c. AD 1305 Kaharoa eruptive episode at Tarawera Volcano, New Zeland. N.Z. J. Geol. Geophys. 44, 467–484.

Nakada, S., Bacon, C.R., Gartner, A.E., 1994. Origin of phenocrysts and compositional diversity in pre-Mazama rhyodacite lavas, Crater Lake, Oregon. J. Petrol. 35, 127–162.

Nakagawa, M., Wada, K., Thordarson, T., Wood, C.P., Gam-

ble, J.A., 1999. Petrologic investigations of the 1995 and 1996 eruptions of Ruapehu volcano, New Zealand: formation of discrete and small magma pockets and their intermittent discharge. Bull. Volcanol. 61, 15–31.

Rogan, A.M., 1982. A geophysical study of the Taupo volcanic zone, New Zealand. J. Geophys. Res. 87, 4073–4088.

Ross, C.S., Smith, R.L., 1961. Ash-flow Tuffs: Their Origin, Geologic Relations, and Identification. U.S. Geol. Surv. Prof. Pap. 366, 81 pp.

Stevenson, R.J., Dingwell, D.B., Bagdassarov, N.S., Manley, C.R., 2001. Measurement and implication of 'effective' viscosity for rhyolite flow emplacement. Bull. Volcanol. 63, 227–237.

Stevenson, R.J., Hodder, A.P.W., Briggs, R.M., 1994. Rheological estimates of rhyolite lava flows from the Okataina Volcanic Centre, New Zealand. N.Z. J. Geol. Geophys. 37, 211–221.

Swanson, S.E., Naney, M.T., Westroch, H.R., Eichelberger, J.C., 1989. Crystallization history of Obsidian Dome, Inyo Domes, California. Bull. Volcanol. 51, 161–176.

Tait, S., 1992. Selective preservation of melt inclusions in igneous phenocrysts. Am. Mineral. 77, 146–155.

Walker, G.P.L., 1973. Lengths of lava flows. Philos. Trans. R. Soc. Lond. 274, 107–118.

Wagner, G.J., Storzer, D., Keller, J., 1976. Spaltspurendatierungen quartärer Gesteinsgläser aus dem Mittelmeerraum. N. Jb. Miner. Mh. Jg. 1976, 84–94.

Wilson, C.J.N., Houghton, B.F., Lloyd, E.F., 1986. Volcanic history and evolution of the Maroa-Taupo area, central North Island. In: Smith, I.E.M. (Ed.), Late Cenozoic Volcanism in New Zealand. R. Soc. N.Z. Bull. 23, 194–223.

Wilson, C.J.N., Houghton, B.F., McWilliams, M.O., Lanphere, M.A., Weaver, S.D., Briggs, R.M., 1995. Volcanic and structural evolution of Taupo Volcanic Zone, New Zealand: a review. J. Volcanol. Geotherm. Res. 68, 1–28.

Wilson, C.J.N., Rogan, A.M., Smith, I.E.M., Northey, D.J., Nairn, I.A., Houghton, B.F., 1984. Caldera volcanoes of the Taupo Volcanic Zone, New Zealand. J. Geophys. Res. 89, 8463–84841.